Creep of lanthanum gallate

William E. Luecke[a)]
Ceramics Division, National Institute of Standards & Technology, Gaithersburg, Maryland 20899
Timothy R. Armstrong
Metals & Ceramics Division, Oak Ridge National Laboratory, Oak Ridge, Tennessee 37831

(Received 21 June 2001; accepted 10 December 2001)

Strontium- and magnesium-doped lanthanum gallate (LSGM) was deliberately prepared to give A-site deficient nonstoichiometry with compositions $(La_{0.9}Sr_{0.1})_z(Ga_{0.8}Mg_{0.2})O_{3-\delta}$ ($z = 1.0$, 0.98, and 0.95). Creep tests in four-point bending for 950 °C < T < 1350 °C and 15 MPa < σ < 75 MPa in air demonstrated that all three compositions shared a common stress dependence, $n = 1.49 \pm 0.10$, and a common apparent activation energy, $Q = 426 \pm 9$ kJ/mol. Despite this agreement, the creep rates of the different compositions depended on grain size in different ways: $p = 3.1 \pm 0.2$ for $z = 0.98$, and $p = 1.9 \pm 0.1$ for $z = 0.95$. The measured apparent activation energy, Q, for creep is similar, though statistically significantly smaller, than that measured in another LSGM. Both are nearly twice as large as reported activation energies for cation impurity diffusion. The absolute magnitude of the creep rates, after correction for grain size, were 30 to 100 times slower than in another LSGM of similar composition.

I. INTRODUCTION

Magnesium- and strontium-doped lanthanum gallate, $(La_{1-x}Sr_x)(Ga_{1-y}Mg_y)O_{3-\delta}$, usually denoted LSGM, is a potential replacement for yttria-doped zirconia as the electrolyte for solid oxide fuel cells because of its high ionic conductivity.[1] Although lanthanum gallate fuel cell electrolytes must survive thousands of hours at elevated temperature under mechanical load, with few exceptions,[2] very little is known about their high-temperature deformation resistance.

The creep behavior of polycrystalline ceramics,[3,4] and perovskites in particular,[5–13] is generally represented by a phenomenological relation between creep rate, $\dot{\epsilon}$, and stress, σ, temperature, T, and grain size, d. Nearly every creep mechanism, whether Nabarro–Herring,[14,15] Coble,[16] or grain boundary sliding (GBS), accommodated by intragranular dislocation motion[17–19] or diffusion[20–23] reduces to

$$\dot{\epsilon} = \frac{A_1}{T}\, d^{-p}\sigma^n \exp\left[-\frac{Q}{RT}\right] \quad , \qquad (1)$$

where n is the stress exponent, Q is the apparent activation energy for creep, p is the grain size exponent, and all the other constants are combined in the prefactor, A_1. It is sometimes possible to differentiate between creep mechanisms by examining the measured values of n, Q, and p.

This manuscript reports results on the creep of LSGM that was processed in an attempt to intentionally produce a lanthanum site deficiency. Other perovskites with lanthanum excess tend to form La_2O_3 which can hydrate in humid environments[24] and degrade mechanical properties. These creep data are interpreted in light of and contrasted with that in the literature,[2] especially with regard to the creep mechanism. Existing theories of creep of doped lanthanum gallate cannot reconcile the differences between the three compositions of this study or those reported in the literature.[2]

II. EXPERIMENTAL PROCEDURE

A. Materials and microstructural characterization

References 25 and 26 detail the processing of the material. Doped powders (Praxair Specialty Ceramics, Woodinville, WA) were sintered in air at 1550 °C for 4 h. [Note: certain commercial equipment, instruments, or materials are identified in this paper to specify the experimental procedure adequately. Such identification is not intended to imply recommendation or endorsement by the National Institute of Standards and Technology, nor is it intended to imply that the materials or equipment identified are necessarily the best available for

a)Address all correspondence to this author.
e-mail: william.luecke@nist.gov

the purpose.] Compositions with three different A:B site stoichiometries were prepared: $(La_{0.9}Sr_{0.1})_z(Ga_{0.8}Mg_{0.2})O_{3-\delta}$, where $z = 1.0$, $z = 0.98$, or $z = 0.95$. To examine the effect of grain size on creep, finished bend-bar specimens were further annealed in air for 70 h at 1550 °C to increase the grain size. Grain sizes were measured by optical microscopy, using the mean linear intercept method,[27] on bend-bar specimens that were thermally etched at 1450 °C for 1 min. To evaluate the mean linear intercept, we measured the actual intercepted width of about 100 grains in each of four randomly selected micrographs. Specimen densities were characterized by Archimedes' method in water. Phase analysis employed x-ray diffraction (Cu K_α radiation, $\lambda = 0.15405945$ nm) using a Siemens D500 diffractometer (Madison, WI) equipped with a focusing Ge incident beam monochromator, sample spinner, and a scanning position-sensitive detector. Patterns were collected from untested bend-bars in the case of the three compositions of this study and from a slab sawed from the billet in the case of the material described in Ref. 2. Use of the position-sensitive detector allowed detection of much smaller second phase peaks than is typically possible.

B. Creep testing

Creep tests in air in the range 950 °C < T < 1350 °C and 15 MPa < σ < 75 MPa employed four-point bending, using B-type[28] (3 × 4 × 45 mm) specimens. The creep fixture has a 40-mm outer span and a 10-mm inner span. The specimen rests on 3.18-mm diameter, nonrolling, cylindrical, sapphire supports. The displacement of the upper load points relative to the lower fixture was measured using an linear variable differential transformer (LVDT) mounted to the crosshead. Thermal expansion errors were nulled using a similarly instrumented rod mounted next to the specimen. A stability test on a nondeforming specimen at typical test temperatures demonstrated that the measured position of the specimen drifted less than 3 μm over 60 h. Generally the segments of the creep curve for determination of a displacement rate were more than 50-μm long and were up to 500 μm, confirming that the error in displacement was generally less than 5% and frequently much less. These load point displacement data were transformed to creep strain by the method of Hollenberg [Eq. (23)][29] using a stress exponent calculated from a multilinear regression of the data for each composition. A specially calibrated B-type thermocouple, mounted less than 7 mm horizontally from the specimen, continuously monitored the test temperature. The reported temperatures are the average temperature during the time over which the strain was measured. Generally, this temperature varied by less than 0.5 °C. A regulated air cylinder that was manually adjusted daily applied the creep load. Generally the stress was constant to within 2 MPa during the test. Usually, specimens were tested at several conditions, in a deliberately random order, to generate data. At each condition, the specimen was allowed to creep until the experimenter deemed load point displacement rate to be constant. Generally after a short transient strain up to $\epsilon = 0.005$ at the start of the test, creep rates at a given condition decreased less than 10% from beginning to end. Tests were terminated at about 4% strain, which is near the point where the tensile face of the specimen touches the lower part of the fixture.

One drawback to flexural creep testing is that if the constitutive laws for deformation are different for tension and compression, the neutral axis of the specimen shifts during creep, which invalidates the Hollenberg[29] analysis. For instance, in structural ceramics like silicon nitride, which have significant fractions of second phase, cavitation and subsequent redistribution of the second phase dominates the tensile creep, while ordinary solution–precipitation of silicon nitride controls creep in compression.[30] The asymmetry in creep response can be quite large: tensile creep of silicon nitride can be thousands of times faster than compression creep, with larger stress exponents and activation energies.[30] This asymmetry makes the methods for extracting the tensile and compressive creep response from flexural creep curves[31–33] complicated and labor intensive. One manifestation of the asymmetry is the appearance of a strong primary creep, as the neutral axis shifts from the center of the specimen to its steady-state position, usually on the compression side of the specimen. Although we did not expect strong asymmetry in creep response, because the LSGM did not have significant second phase, we characterized the neutral axis position of a specimen using the method of Chen.[32] Here the local strain across the specimen is monitored by measuring the separation of a row of indents on the side of the specimen. The test employed rather severe conditions (1200 °C, 37 MPa on the $z = 0.95$ composition to approximately 2% strain) to maximize the possible asymmetry between tension and compression. However, the neutral axis shifted only 130 μm toward the compression side. This is a small shift for the most serious conditions; the reported flexural creep rates may slightly *over*predict the corresponding compressive rates.

III. RESULTS

A. Microstructural characterization

The first five columns of Table I summarize the densities and grain sizes for the three compositions. The grain sizes are reported as the mean linear intercept lengths, L, rather than the three-dimensional grain sizes, d. In addition, the table shows the relative standard deviation [$s(L)/L$] of each distribution of intercept lengths. For the $z = 0.95$ and $z = 0.98$ compositions,

TABLE I. Microstructure data and fitted creep parameters for the three compositions and the data of Wolfenstine.[2]

Material	Density (% theo.)[d]	Grain size $\bar{L}$ (μm)	$s(\bar{L})/\bar{L}$[a]	N_i[b]	$\log_e A_2$ (1/s)	n[c]	Q (kJ/mol)
				Fitted values using Eq. (2)			
$z = 1.0$	92	19.6	0.36	297	23.18 ± 1.72	1.50 ± 0.19	447 ± 20
$z = 0.98$	88	4.3	0.44	362	27.06 ± 1.70	1.45 ± 0.21	452 ± 17
$z = 0.98$		16.2	0.45	449	21.48 ± 3.10	1.76 ± 0.36	447 ± 37
$z = 0.95$	98	7.3	0.47	410	21.84 ± 1.37	1.25 ± 0.17	408 ± 16
$z = 0.95$		21.2	0.44	413	17.08 ± 1.36	1.56 ± 0.18	390 ± 16
Ref. 2[e]	88–92	8.1[f]			33.71 ± 1.48	1.28 ± 0.08	537 ± 19
				Fitted values using Eq. (8)			
				p	$\log_e A_1$		
$z = 0.98$				3.1 ± 0.2	−11.63 ± 1.30	1.60 ± 0.21	449 ± 19
$z = 0.95$				1.9 ± 0.1	−1.56 ± 0.94	1.37 ± 0.12	401 ± 11
				Complete data set $N = 70$ points			
						1.49 ± 0.10	426 ± 9

[a]Estimated relative standard deviation of distribution of intercept lengths.
[b]Number of intercepts measured.
[c]Uncertainties listed are the standard uncertainties (estimated standard deviations) of the parameters.
[d]Assuming a theoretical density of 6698 kg/m^3, calculated from a lattice parameter, $a_0 = 0.3917$ nm.[34]
[e]$La_{0.8}Sr_{0.2}Ga_{0.85}Mg_{0.15}O_{2.825}$.
[f]Reported values.

grain growth did not change the shape of the distribution of mean linear intercept lengths. By visual inspection, the grains of all compositions were equiaxed. The measured grain sizes differ slightly from those in an earlier study,[25] which came from specimens of a different powder lot and were reported as $d = 1.5\,L$. Specimens in this study with $z = 0.98$ and $z = 1.0$ were not fully dense, evaluated quantitatively by Archimedes' method and qualitatively by the numerous pores visible in the micrographs of polished surfaces used for the grain size analysis. These pores were concentrated at triple junctions in three original compositions. The second grain growth anneal for the $z = 0.98$ and $z = 0.95$ compositions increased both the pore and grain sizes and trapped some smaller pores inside the grains.

Figure 1, which shows x-ray diffraction traces from the three compositions and the $La_{0.8}Sr_{0.2}Ga_{0.85}Mg_{0.15}O_{2.825}$ of Ref. 2, confirms their excellent phase-purity. Table II summarizes the peak positions and intensities. Although each composition contains identifiable secondary phases, their volume fraction is very small: the largest of the second phase peaks is only 1.5% of the main LSGM peak, and the other peaks are only 1/10 as large. None of these second phase peaks correspond to any of the usual second phases in LSGM, such as $LaSrGaO_4$,[26,34] $La_4Ga_2O_9$,[35] $SrLaGa_3O_7$,[26,34] or $Sr_3Ga_2O_6$.[35] Although Stevenson *et al.*[26] reported MgO in the similar LSGM of the study before this one, none of the peaks in Fig. 1 are unambiguously consistent with MgO. The large background at low angles probably arises from scattering from the plastic specimen holder.

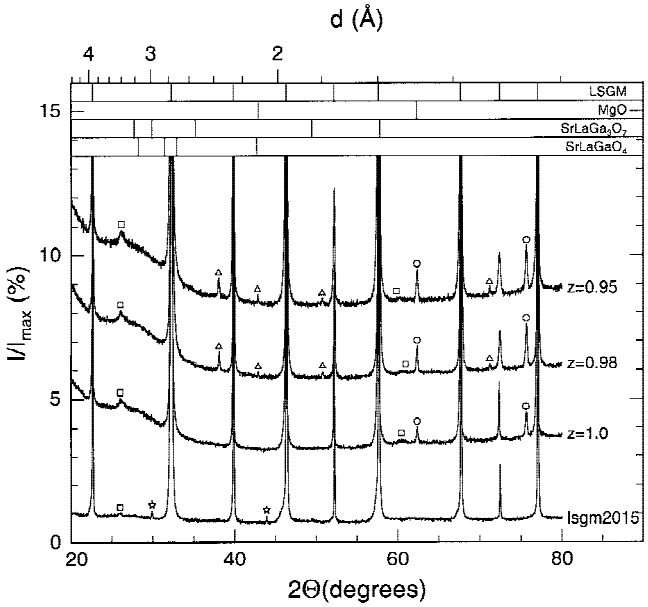

FIG. 1. X-ray diffraction traces from the three compositions and for the material of Ref. 2 (labeled lsgm2015). The symbols identify possible different secondary phases. Note that the largest second phase peak is only 1.5% as large at the main LSGM peak. The bands across the top denote the major peak positions of doped lanthanum gallate[34] (LSGM) and some common secondary phases.

We have assigned the second phase peaks to four groups. The strongest peaks at $d = 1.487$ Å and $d = 1.256$ Å appear in all three compositions of this study, but not in the LSGM of Ref. 2. A set of four tiny ($I/I_{max} < 0.5\%$) peaks appears in both of the A-site

TABLE II. Peak heights and positions from the x-ray traces in Fig. 1.

$z = 1.0$		$z = 0.98$		$z = 0.95$		LSGM2015[2]	
d (Å)	I/I_{max} (%)	d (Å)	I/I_{max} (%)	d (Å)	I/I_{max} (%)	d (Å)	I/I_{max} (%)
			$(La_{1-x}Sr_x)(Ga_{1-y}Mg_y)O_{3-\delta}$				
3.9212	8.7	3.9142	10.8	3.9210	9.8	3.9143	8.3
2.7710	100.0	2.7661	100.0	2.7694	100.0	2.7661	100.0
2.2619	18.0	2.2598	10.5	2.2620	11.3	2.2587	15.3
1.9586	26.6	1.9554	36.3	1.9578	31.3	1.9554	26.4
1.7516	4.8	1.7491	4.0	1.7503	4.1	1.7491	4.6
1.5990	42.6	1.5980	25.6	1.5990	28.2	1.5965	38.7
1.3847	13.4	1.3826	10.4	1.3833	10.9	1.3826	14.1
1.3052	2.0	1.3043	1.3	1.3043	1.5	1.3034	1.9
1.2383	11.5	1.2366	9.9	1.2372	9.8	1.2366	11.6
			Unknown phase 1 (○)[a]				
1.4870	0.6	1.4874	1.0	1.4874	1.1		
1.2563	0.8	1.2557	1.5	1.2554	1.6		
			Unknown phase 2 (Δ)				
		2.3601	0.8	2.3625	1.1		
		2.1056	0.2	2.1092	0.3		
		1.7952	0.3	1.7972	0.3		
		1.3224	0.1	1.3233	0.2		
			Unknown phase 3 (□)				
3.4220	0.2	3.4139	0.4	3.4166	0.5	3.4063	0.1
1.5302	0.1	1.5297	0.1	1.5359	0.1	N/d	
			Unknown phase 4 (☆)				
						2.9842	0.3
						2.0599	0.3

[a]Symbol assignments refer to Fig. 1.

deficient materials ($z = 0.98$ and $z = 0.95$) but not in the stoichiometric composition ($z = 1.0$). All four compositions have two broad peaks, suggesting a second phase with extremely fine particle size. The LSGM of Ref. 2, whose phase purity is slightly greater than the three compositions of this study, has two unidentified peaks that do not appear in the other specimens. One ($d = 2.984$ Å) corresponds to the largest peak for $SrLaGa_3O_7$, but the other ($d = 2.0599$ Å) is not from that phase.

B. Creep

Figure 2 shows a typical creep curve for the $z = 1.0$ composition at 1225 °C. The primary creep that occurs when the load is first applied represents a 2× reduction in strain rate, but the transition to the new creep rate after the stress increase was nearly immediate, a behavior common to all the specimens. The mild primary creep should be contrasted with the 20× reduction in creep rate for a silicon nitride that has significant tension/compression asymmetry.[32] Table III summarizes the creep data of this study, and Fig. 3 compares the secondary creep rate data as a function of stress and temperature for the three compositions. The creep rates were highly repeatable. Table III has six replicated conditions. The largest difference is only 50%, and 20% difference is typical. There is no correlation between the sign of the difference and the order of the determination, indicating that primary creep is probably not significant.

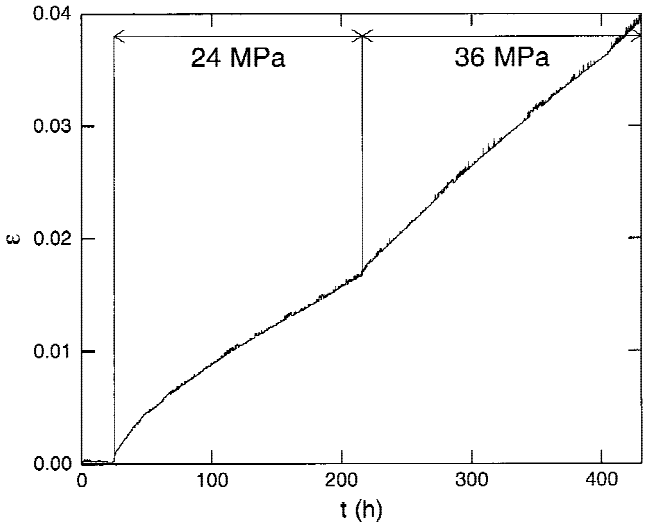

FIG. 2. Typical creep curve for the $z = 1.0$ composition at 1125 °C.

IV. DISCUSSION

The discussion of the results of this study comprises three parts. First we will use the creep rate data to calculate the apparent grain size exponent, p. Then, we shall

compare the data of this study to existing creep data for another composition of LSGM and discuss the origins of the differences. Finally, we shall discuss the creep parameters (Q, n, and p) in light of existing creep theories.

For the case of unknown grain size, Eq. (1) can be simplified by folding the grain size exponent, p, into the prefactor, A_1:

$$\dot{\epsilon} = \frac{A_2}{T}\,\sigma^n \exp\left[-\frac{Q}{RT}\right] \quad . \tag{2}$$

The data of Fig. 3 for the individual compositions give no indication that the apparent activation energy and stress exponent depend on temperature or stress, as others have observed in various perovskites.[6,12,13] Accordingly, the last three columns of Table I show the fits of the natural logarithm of Eq. (2) to the individual data sets. The apparent activation energies and stress exponents are quite similar even across grain size and composition.

We can evaluate the grain size exponent, p, for the $z = 0.98$ and $z = 0.95$ compositions. If the grain size exponent is to be interpreted in the light of standard creep models, it is necessary that the other creep parameters (n and Q) be unchanged by the grain growth. The statistical test outlined in the Appendix demonstrates that this is the case for both compositions. A second problem in using the natural logarithm of Eq. (1) to evaluate the grain size exponent, p, is that the data in Table I are for the mean linear intercept length, L, and not the three-dimensional grain size, d. Some work in this area[27] indicates that d is linearly proportional to L. When the distribution of

TABLE III. Creep rate data for the three compositions.

$z = 1.0$, $\bar{L} = 19.6$ μm				$z = 0.98$, $\bar{L} = 4.3$ μm				$z = 0.95$, $\bar{L} = 7.3$ μm			
T (°C)	σ (MPa)	$\dot{\epsilon}$ (1/s)	Spec. ID[a]	T (°C)	σ (MPa)	$\dot{\epsilon}$ (1/s)	Spec. ID	T (°C)	σ (MPa)	$\dot{\epsilon}$ (1/s)	Spec. ID
1102	38	2.6×10^{-8}	15–5	998	52	3.3×10^{-8}	1–4	951	50	1.1×10^{-9}	8–3
1125	24	2.1×10^{-8}	16–1	1000	24	1.2×10^{-8}	2–6	1001	49	8.4×10^{-9}	8–2
1125	36	2.8×10^{-8}	16–2	1000	38	2.3×10^{-8}	2–2	1001	73	6.7×10^{-9}	8–12
1150	25	4.8×10^{-8}	15–3	1050	25	1.0×10^{-7}	1–1	1003	73	8.5×10^{-9}	8–9
1175	15	3.0×10^{-8}	14–2	1054	36	1.4×10^{-7}	2–1	1051	49	2.3×10^{-8}	8–4
1175	23	5.9×10^{-8}	14–1	1050	52	2.1×10^{-7}	1–2	1052	72	3.8×10^{-8}	8–11
1175	24	5.3×10^{-8}	14–3	1103	22	1.7×10^{-7}	1–5	1099	23	3.8×10^{-8}	8–1
1179	49	2.3×10^{-7}	17–4	1101	49	7.3×10^{-7}	1–3	1099	48	9.6×10^{-8}	9–1
1200	26	1.4×10^{-7}	15–2	1151	24	1.2×10^{-6}	2–5	1100	49	7.7×10^{-8}	8–5
1203	50	3.7×10^{-7}	17–5	1151	37	1.9×10^{-6}	2–3	1100	74	1.3×10^{-7}	8–10
1226	44	7.2×10^{-7}	11–1	1151	50	3.3×10^{-6}	2–4	1149	20	6.1×10^{-8}	8–6
1250	25	7.8×10^{-7}	15–1					1149	48	2.8×10^{-7}	8–7
1249	37	5.5×10^{-7}	15–4					1149	73	4.8×10^{-7}	8–8
1274	23	6.9×10^{-7}	17–2								
1276	25	7.2×10^{-7}	17–3								
1274	37	1.3×10^{-6}	17–1								

$z = 0.98$, $\bar{L} = 16.2$ μm				$z = 0.95$, $\bar{L} = 21.2$ μm			
T (°C)	σ (MPa)	$\dot{\epsilon}$ (1/s)	Spec. ID	T (°C)	σ (MPa)	$\dot{\epsilon}$ (1/s)	Spec. ID
1150	28	3.2×10^{-8}	1–11	1149	28	2.4×10^{-8}	2–14
1153	39	7.2×10^{-8}	1–13	1155	37	2.2×10^{-8}	2–3
1150	49	4.8×10^{-8}	1–5	1150	51	5.4×10^{-8}	2–12
1201	24	5.0×10^{-8}	1–1	1152	52	4.7×10^{-8}	1–1
1202	24	3.4×10^{-8}	1–7	1200	25	3.4×10^{-8}	2–11
1201	35	8.8×10^{-8}	1–2	1200	38	7.3×10^{-8}	2–9
1201	50	1.8×10^{-7}	1–6	1250	24	8.9×10^{-8}	2–4
1251	28	2.6×10^{-7}	1–10	1250	31	2.5×10^{-7}	2–13
1251	33	2.2×10^{-7}	1–3	1250	38	1.8×10^{-7}	2–2
1251	50	4.6×10^{-7}	1–4	1250	50	3.0×10^{-7}	2–5
1301	21	4.5×10^{-7}	1–8	1300	23	2.9×10^{-7}	1–1
1301	33	1.5×10^{-6}	1–12	1300	23	2.3×10^{-7}	2–6
1301	50	2.4×10^{-6}	1–9	1300	37	5.8×10^{-7}	2–8
				1300	49	6.9×10^{-7}	2–1
				1300	50	8.7×10^{-7}	2–10
				1300	52	1.1×10^{-6}	1–2
				1350	35	1.4×10^{-6}	2–7

[a]Spec. ID differentiates the data by specimen and run order within a composition. For example, 15–2 designates the 2nd set of test conditions in specimen 15.

intercept lengths is unchanged by grain growth (as is the case in this study; see Table I), then the proportionality constant is the same for both grain sizes. Then, the constant can be absorbed into the prefactor, A_1, and no information is lost by assuming $d = L$. Table I shows the grain size exponents evaluated by a multilinear regression of the natural logarithm of Eq. (1) on the full data sets for the $z = 0.98$ and $z = 0.95$ compositions. The Appendix details the calculation. Interestingly, although the two compositions have statistically indistinguishable stress and temperature dependencies, and identical phase compositions (Fig. 1), the grain size exponent for the $z = 0.98$ composition is significantly larger than that for the $z = 0.95$ composition: $p_{0.98} = 3.1 \pm 0.2$ versus $p_{0.95} = 1.9 \pm 0.1$.

The analysis described above, which showed that n and Q are not statistically significantly different for the two grain sizes of the $z = 0.98$ and $z = 0.95$ compositions, can be further generalized to show that the five sets of data in Table III share a common stress dependence and activation energy: $n = 1.49 \pm 0.10$ and $Q = 426 \pm 9$ kJ/mol. All of the prefactors, A_2, in Eq. (2) are different, however.

Recently, Wolfenstine *et al.*,[2,8] reported compressive creep data for LSGM of a slightly different composition (LSGM2015: $La_{0.8}Sr_{0.2}Ga_{0.85}Mg_{0.15}O_{2.825}$), comparable grain size, and slightly higher phase-purity (see Fig. 1). Table I shows that the activation energy for creep, $Q = 537 \pm 19$ kJ/mol, is statistically significantly larger than that of this study. [Wolfenstine[2] originally reported 521 ± 23 kJ/mol, which he evaluated using a form of Eq. (2) without the leading $1/T$.] In addition, they measured a grain size exponent, $p = 1.7 \pm 0.1$ for $8.1\ \mu m < L < 14\ \mu m$, and demonstrated that the creep rate was independent of oxygen activity.

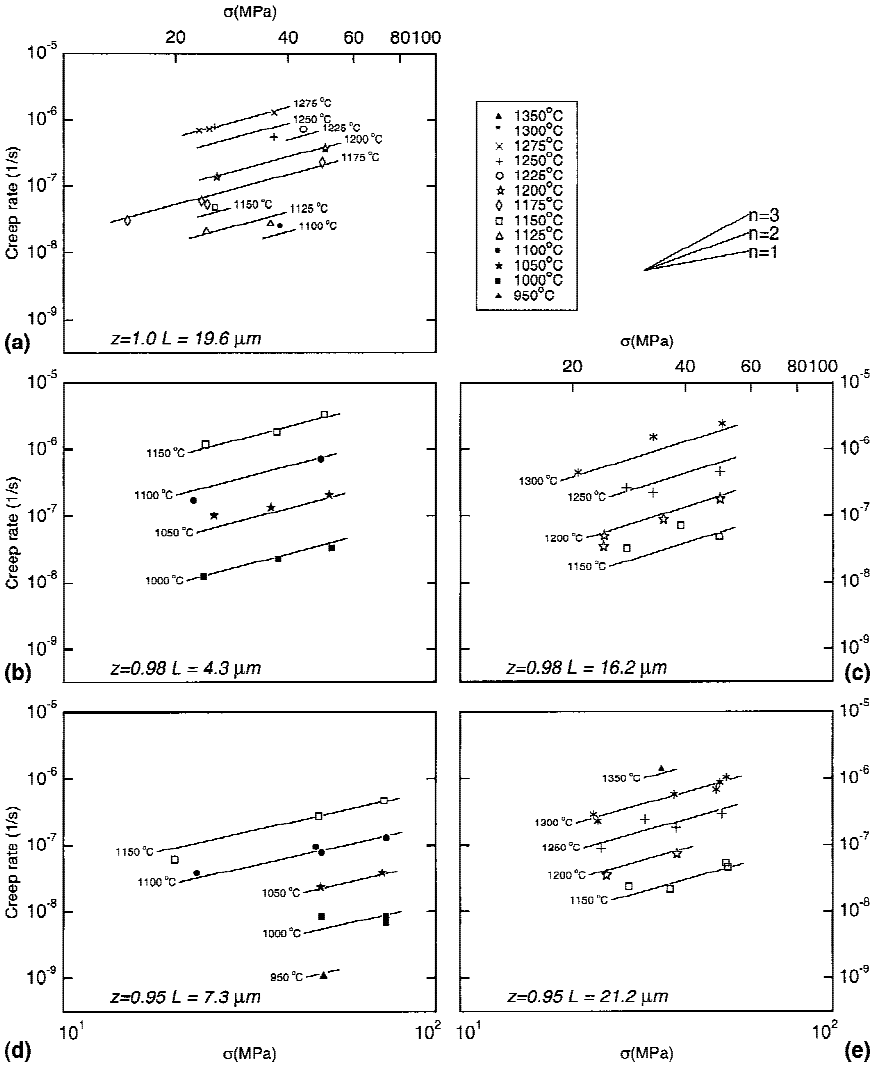

FIG. 3. Creep data for the three compositions: (a) $z = 1.0$ (5 specimens); (b) $z = 0.98$, $\bar{L} = 4.3\ \mu m$ (2 specimens); (c) $z = 0.98$, $\bar{L} = 16.2\ \mu m$ (1 specimen); (d) $z = 0.95$, $\bar{L} = 7.3\ \mu m$ (2 specimens); (e) $z = 0.95$, $\bar{L} = 21.2\ \mu m$ (2 specimens). Note the different temperature ranges. Solid lines are from the fits of the natural logarithm of Eq. (2), summarized in Table I.

In addition to the difference in grain size exponents and smaller activation energy, the data of this study also differ from that of Wolfenstine[2] in one other significant way. The absolute values their creep rates, corrected for grain size, are 30 and 100 times faster. Figure 4 compares the creep rates, evaluated at two different grain sizes, for the material of this study and of Wolfenstine.[2] For each composition ($z = 0.95$ and $z = 0.98$), the rates were calculated using the appropriate grain size exponent, p, summarized in Table I.

Simple temperature or stress differences between the laboratories cannot explain the enormous difference in creep rates between the studies. For instance, the temperature correction between the two studies necessary to harmonize the two sets of data is greater than 100 °C, an obvious impossibility. Furthermore, interlaboratory comparison between the laboratory of Wolfenstine *et al.* and another laboratory[36] has yielded excellent agreement, indicating that the absolute temperatures cannot be substantially different. We have also demonstrated excellent interlaboratory repeatability[37] in creep testing using the same temperature measurement protocols as this study. The possibility of small neutral axis shift in the flexural creep measurements cannot reconcile the difference either, since significant neutral axis shift would tend to *over*predict the corresponding compressive creep rate.

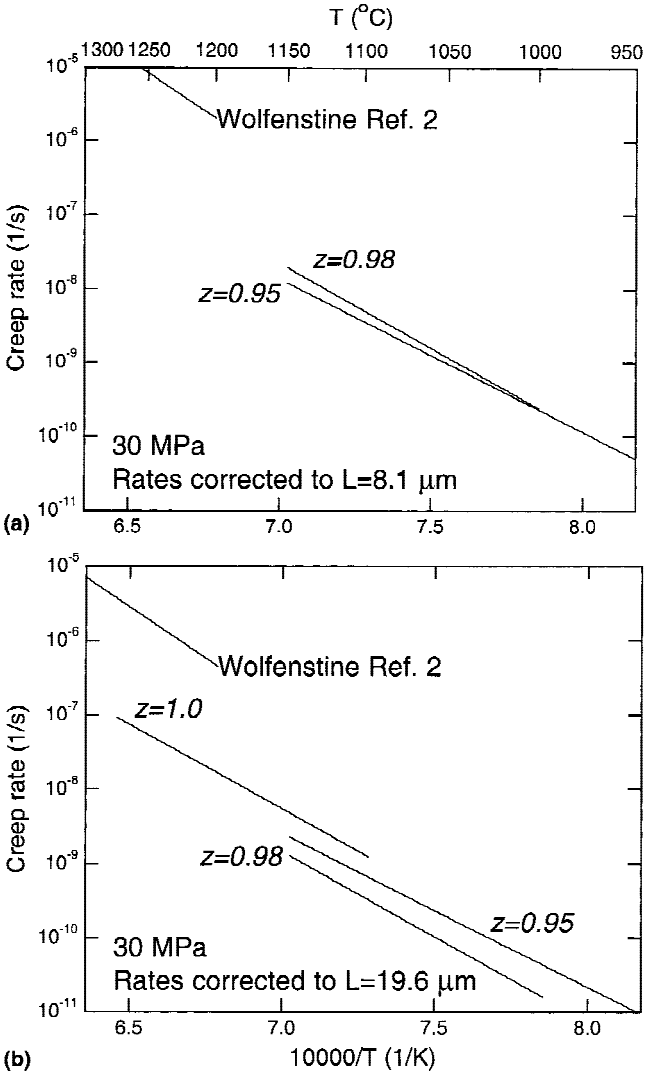

FIG. 4. Comparison of the creep rates at 30 MPa for the three compositions and the LSGM of Wolfenstine[2] evaluated using the fits of Eq. (1), including the individual grain size exponents, p, for each composition, summarized in Table I. The rates are presented at two grain sizes: $L = 8.1$ μm, the grain size of the material of Ref. 2, and $L = 19.6$ μm, the grain size of the $z = 1.0$ composition.

One purpose in measuring the creep parameters is to gain insight into the creep mechanism of LSGM. Dozens of diffusional creep models for ceramics have been developed over the past 30 years (see for example Hynes and Doremus[4]). Models in which intragranular dislocation slip produces the strain[18,19] have not been extensively applied to ceramics because dislocations are not often observed. The traditional diffusional creep models (Nabarro–Herring[14,15] and Coble[16]) as well as models involving grain rotation or sliding[22,23] all predict $n = 1$ and $p = 2$ or $p = 3$ when diffusion limits the creep rate. For deformation to occur in diffusional creep, entire unit cells of the compound must be transported down the stress gradient. For a multicomponent oxide, the transport of the slowest individual species on its fastest path controls the creep rate. In an ABO_3 perovskite, this could be the A- or B-site cation or oxygen. In their simplest form these models all assume that the grain boundary is an infinite source and sink for point defects. The Ashby–Verrall model[22] assumes that point defects are created and destroyed on climbing grain boundary dislocations. Arzt[21] has treated the analogous case for the Nabarro–Herring[14,15] and Coble[16] creep. Only when these dislocations have high mobility does the diffusion of point defects control the creep rate. In the case of limited dislocation mobility, the creep rate can become "interface-reaction controlled," and then $n = 2$ and $p = 1$; the extra stress term arises from the assumed increase in grain boundary dislocation density with stress. Between the two limiting behaviors, the stress exponent takes on values $1 < n < 2$ and the grain size exponent $2 > p > 1$. The apparent activation energy is a mixture of that for point defect diffusion and that for dislocation mobility. Small grain sizes favor interface reaction control.[22] In this case, the activation energy for creep is that for the mechanism that controls the grain boundary dislocation mobility. For instance, solute drag may control the dislocation motion.[21]

Wolfenstine[2] has argued that grain boundary sliding[20] accommodated by lattice diffusion of cation, rather than oxygen, vacancies, which has a theoretical stress and grain size exponents, $n = 1$ and $p = 2$, controls creep of coarse-grained lanthanum gallate. Other

coarse-grained perovskites, exhibit this dependence, while fine-grained perovskites exhibit $p \approx 1$ [$BaTiO_3$[11] ($19.3\ \mu m < L < 52.4\ \mu m$, $p = 1.8 \pm 0.2$, $n = 1.1 \pm 0.2$); $CaTiO_3$[5] ($6.3\ \mu m < L < 18.2\ \mu m$, $p \approx 2$, $n \approx 1$); $CaTiO_3$[6] ($2\ \mu m < L < 7\ \mu m$, $p = 1$, $n = 1$); $Sr(Co,Fe)O_3$[13] ($2.4\ \mu m < L < 7.3\ \mu m$, $1 < n < 1.45$, $p = 1$)]. In addition to the correspondence with the theoretical stress and grain size exponents, the measured activation energy for creep was nearly 10 times that for oxygen tracer diffusion in LSGM: 61 to 71 kJ/mol.[38] He further noted that theoretical calculations[39] predict high activation energies for lanthanum vacancy (386 kJ/mol) and gallium vacancy (1600 kJ/mol) diffusion. However, recent cation impurity diffusion measurements of Y, Cr, and Fe by Schulz *et al.*[40,41] yield activation energies of 200 to 250 kJ/mol in the range 900 °C < T < 1400 °C, which are only half that measured in both this study and by Wolfenstine.[2]

The results of the grain size exponent analysis are difficult to integrate into a complete model. On one hand the $z = 0.98$ and $z = 0.95$ compositions have identical phase compositions (Fig. 1) and their creep rates have statistically indistinguishable temperature and stress dependencies. Both facts point toward identical creep mechanisms. On the other hand, their creep rates depend on grain size in statistically significantly different ways ($p_{0.98} = 3.1 \pm 0.2$ versus $p_{0.95} = 1.9 \pm 0.1$), which points to different deformation mechanisms for each: for example, a grain boundary diffusion limited (Coble[16]) mechanism for the $z = 0.98$ composition and a bulk-diffusion-limited mechanism[14,15,22,23] for the $z = 0.95$ composition. The smaller grain size of the $z = 0.98$ composition would favor this assignment, but the grain size ranges of the two compositions are not wildly different. However, existing creep data on perovskites indicates that interface-reaction control[21,22] (with $n = 2$ and $p = 1$) is more common at small grain sizes.[6,13] In any case, the impurity lattice diffusion data of Schulz and Martin[40,41] are evidence against a cation lattice diffusion controlled mechanism. Finally, it would be extremely unusual that two different mechanisms would share a common stress exponent and activation energy.

The magnitude of the difference in creep rates between the two studies is also incommensurable with Wolfenstine's[2] model for the rate-controlling species. That model predicts an inverse 3/2 dependence of creep rate on dopant fraction, which should make the LSGM of that study creep about 1.25 times *more* slowly rather than 30–100 times faster (Fig. 4).

The difference in activation energies between this study, that of Wolfenstine,[2] and the diffusion data of Schulz and Martin,[40] as well as the enormous difference in absolute rates between this study and Wolfenstine,[2] point to a more complicated creep mechanism than Wolfenstine originally envisioned from his creep data. Nothing in this study points to an obvious origin of the differences in the two studies, however. In the absence of confirming data, any argument for alternate mechanisms would be speculative at best. At this time, we must regard the origin of the differences between the two studies as unresolved.

V. SUMMARY

Three compositions and two grain sizes of $(La_{0.9}Sr_{0.1})(Ga_{0.8}Mg_{0.2})O_{3-\delta}$, deliberately prepared in an attempt to give A-site nonstoichiometry, exhibit a common stress dependence and apparent activation energy: $n = 1.49 \pm 0.10$ and $Q = 426 \pm 9$ kJ/mol. Despite this agreement, the creep rates for the different compositions depend on grain size in statistically significantly different ways: $p = 3.1 \pm 0.2$ for $z = 0.98$ and $p = 1.9 \pm 0.1$ for $z = 0.95$. The measured activation energy for creep is inconsistent with a model for creep controlled by cation vacancy diffusion. The absolute magnitudes of the creep rates, after correction for grain size, are 30 to 100 times slower than previously measured creep rates in a lanthanum gallate of similar, but not identical, composition. The origin of these differences is unresolved.

ACKNOWLEDGMENTS

W.E. Luecke acknowledges the persistence of Ralph Krause, Jr., in demanding correct statistical tests, and James Cline and Mark Vaudin for assistance collecting the x-ray data. Jeff Wolfenstine kindly provided the specimen of material from Ref. 2.

REFERENCES

1. T. Ishihara, H. Matsuda, and Y. Takita, J. Am. Chem. Soc. **116,** 3801 (1994).
2. J. Wolfenstine, Solid State Ionics **126,** 293 (1999).
3. W.R. Cannon and T.G. Langdon, J. Mater. Sci. **18,** 1 (1983).
4. A. Hynes and R. Doremus, Crit. Rev. Solid State Mater. Sci. **21,** 129 (1996).
5. P. Li, S-I. Karato, and Z. Wang, Phys. Earth Planet. Inter. **95,** 19 (1996).
6. H. Yamada, J. Mater. Sci. **19,** 2639 (1984).
7. J.L. Routbort, K.C. Goretta, R.E. Cook, and J. Wolfenstine, Solid State Ionics **129,** 53 (2000).
8. J. Wolfenstine, P. Huang, and A. Petric, J. Electrochem. Soc. **147,** 1668 (2000).
9. R.E. Cook, K.C. Goretta, J. Wolfenstine, P. Nash, and J.L. Routbort, Acta Mater. **47,** 2969 (1999).
10. J. Wolfenstine, K.C. Goretta, R.E. Cook, and J.L. Routbort, Solid State Ionics **92,** 75 (1996).
11. E.T. Park, P. Nash, J. Wolfenstine, K.C. Goretta, and J.L. Routbort, J. Mater. Sci. **14,** 523 (1999).
12. C. Carry and A. Mocellin, J. Am. Ceram. Soc. **69,** C215 (1986).
13. G. Majkic, L. Wheeler, and K. Salama, Acta Mater. **48,** 1907 (2000).
14. F.R.N. Nabarro, in *Report of a Conference on Strength of Solids* (Physical Society) (Great Britain, 1948), pp. 75–90.

15. C. Herring, J. Appl. Phys. **21,** 437 (1950).
16. R.L. Coble, J. Appl. Phys. **34,** 1679 (1963).
17. T.G. Langdon, Acta Metall. Mater. **42,** 2437 (1994).
18. O.A. Ruano, J. Wadsworth, J. Wolfenstine, and O.D. Sherby, Mater. Sci. Eng. A **A165,** 133 (1993).
19. R.C. Gifkins, Metall. Trans. A **7A,** 1225 (1976).
20. R. Raj and M.F. Ashby, Metall. Trans. **2,** 1113 (1971).
21. E. Arzt, M.F. Ashby, and R.A. Verrall, Acta Metall. **31,** 1977 (1983).
22. M.F. Ashby and R.A. Verrall, Acta Metall. **21,** 149 (1973).
23. J.N. Wang, Acta Mater. **48,** 1517 (2000).
24. C.P. Khattak and D.E. Cox, Mater. Res. Bull. **12,** 463 (1977).
25. S. Baskaran, C.A. Lewinsohn, Y-S. Chou, M. Qian, J.W. Stevenson, and T.R. Armstrong, J. Mater. Sci. **34,** 3913 (1999).
26. J.W. Stevenson, T.R. Armstrong, L.R. Pederson, J. Li, C.A. Lewinsohn, and S. Baskaran, Solid State Ionics **113–115,** 571 (1998).
27. M.I. Mendelson, J. Am. Ceram. Soc. **52,** 443 (1969).
28. Standard Test Method for Flexural Strength of Advanced Ceramics at Ambient Temperature, Standard C1161-94, *Annual Book of ASTM Standards* (American Society for Testing and Materials, 1998), Vol. 15.01.
29. G.W. Hollenberg, G.R. Terwilliger, and R.S. Gordon, J. Am. Ceram. Soc. **54,** 196 (1971).
30. K.J. Yoon, S.M. Wiederhorn, and W.E. Luecke, J. Am. Ceram. Soc. **83,** 2017 (2000).
31. T-J. Chuang, J. Am. Ceram. Soc. **81,** 2749 (1998).
32. C-F. Chen and T-J. Chuang, J. Am. Ceram. Soc. **73,** 2366 (1990).
33. T-J. Chuang, J. Mater. Sci. **21,** 165 (1986).
34. K. Huang, R.S. Tichy, and J.B. Goodenough, J. Am. Ceram. Soc. **81,** 2565 (1998).
35. E. Djurado and M. Labeau, J. Eur. Ceram. Soc. **18,** 1397 (1998).
36. J.L. Routbort, K.C. Goretta, A.R. de Arellano López, and J. Wolfenstine, Scr. Mater. **38,** 315 (1998).
37. W.E. Luecke and S.M. Wiederhorn, J. Am. Ceram. Soc. **80,** 831 (1997).
38. T. Ishihara, J.A. Kilner, M. Honda, N. Sakai, H. Yokokawa, and Y. Takita, Solid State Ionics **113–115,** 593 (1998).
39. M.S. Khan, M.S. Islam, and D.R. Bates, J. Phys. Chem. B **102,** 3099 (1998).
40. O. Schulz and M. Martin, Solid State Ionics, **135,** 549 (2000).
41. O. Schulz and M. Martin, in *Mass and Charge Transport in Inorganic Materials: Fundamentals to Devices*, No. 29 in Advances in Science and Technology, edited by P. Vincenzini and V. Buscaglia (Techna, Faenza, Italy, 2000), pp. 83–90.
42. W. Mendenhall and T. Sincich, Statistics for Engineering and the Sciences (Dellen Publishing Company, New York, 1992), Chap. 13.

APPENDIX

We would like to evaluate the grain size exponent, p, from the entire data set for a composition, encompassing two grain sizes, and multiple temperatures and stresses rather than using the traditional method of comparing creep rates at a limited number of fixed conditions. If the grain size exponent is to have physical meaning, we must first ensure that the stress and temperature dependencies between the two grain sizes are the same. We can rewrite Eq. (2) as

$$T\dot{\epsilon} = A_2\sigma^n \exp\left[-\frac{Q}{RT}\right] \quad . \tag{3}$$

We will use analysis of variance for regression, described by Mendenhall,[42] to compare two linear regression models. The first, or complete, regression model assumes that each grain size for a given composition has distinct A, n, and Q values for a total of 6 independent parameters. The second, or reduced, regression model assumes that some of the parameters in the complete model are zero; i.e., they do not contribute to the fit. We can form any number of reduced models to test which parameters are significant, using an F-test to compare the reduction in the sum of squares for error between the complete and reduced regression model to that of the complete regression model, with the hypothesis that all of the extra terms in the complete regression model are zero. If the reduction in error is small, the omitted terms did not contribute to the complete regression model. Both the complete and reduced regression models use all of the data for a given composition listed in Table III: $N = 24$ points for $z = 0.98$, and $N = 30$ points for $z = 0.95$.

The complete model for the case of two grain sizes is written

$$\log_e(T\dot{\epsilon}) = \left(\log_e A_S + n_S \log_e \sigma - \frac{Q_S}{RT}\right) + x_L\left(\log_e A'_L + n'_L \log_e \sigma - \frac{Q'_L}{RT}\right) \quad , \tag{4}$$

where the subscripts S and L refer to the small and large grain sizes respectively. The variable x_L is a dummy such that $x_L = 1$ for the large grain size and zero otherwise. Table IV shows the results of the linear regression of Eq. (4) for the complete model for both grain sizes. After some manipulation of the individual terms, the parameters of this regression are the same as those from the fits of the natural logarithm of Eq. (2) to the individual data sets, which Table I reports. For example for the $z = 0.98$ composition $Q_L = Q_S + Q'_L$.

Examining the standard uncertainties (estimated standard deviations) of the parameters in the complete model (Table IV) indicates that two of them (n'_L and Q'_L) do not contribute to the fit. We can write a reduced regression model

$$\log_e(T\dot{\epsilon}) = \log_e A_S + n \log_e \sigma - \frac{Q}{RT} + x_L \log_e A'_L \quad , \tag{5}$$

which assumes that the two grain sizes share a common n and Q but differ in the prefactor, A. Of course the difference in the prefactors A_S and A_L arise from the assumed grain size exponent. Table IV shows the results of those regressions as well. To test our hypothesis we calculate the F-statistic

$$F = \frac{(\mathrm{SSE_r} - \mathrm{SSE_c})/(k-g)}{\mathrm{SSE_c}/[N-(k+1)]} \quad , \tag{6}$$

TABLE IV. Results of the regression analyses of Eqs. (4) and (5) to determine the nonzero parameters of the complete and reduced models.

		$z = 0.98$					
Model	SSE[a]	A'_L	A_S	n'_L	n_S	Q'_L	Q_S
Complete (Eq. 4)	1.87	−5.56 ± 3.58	27.05 ± 2.45	0.30 ± 0.43	1.45 ± 0.30	5 ± 40	452 ± 25
		A'_L	A_S	n		Q	
Reduced (Eq. 5)	1.93	−4.07 ± 0.21	26.30 ± 1.79	1.60 ± 0.21		449 ± 19	
		$z = 0.95$					
	SSE	A'_L	A_S	n'_L	n_S	Q'_L	Q_S
Complete (Eq. 4)	1.21	−4.76 ± 1.93	21.85 ± 1.33	0.32 ± 0.25	1.25 ± 0.16	−19 ± 23	409 ± 16
		A'_L	A_S	n		Q	
Reduced (Eq. 5)	1.36	−2.01 ± 0.14	20.74 ± 1.02	1.37 ± 0.12		401 ± 11	

[a]SSE = sum of squares for error, Eq. (7).

where the subscripts r and c refer to the reduced and complete models, respectively, and SSE is the sum of squares for error of the fit.

$$\mathrm{SSE} = \sum_{i=1}^{N} [\log_e(T\dot{\epsilon}_i) - \widehat{\log_e(T\dot{\epsilon}_i)}]^2 \quad , \qquad (7)$$

where the hat designates the fitted value. There are $k + 1 = 6$ and $g + 1 = 4$ parameters in the complete and reduced model. Testing a reduced model with fewer parameters than in Eq. (5) for either the $z = 0.98$ or $z = 0.95$ composition yields *F*s that are significant at the 95% probability level, indicating that the parameters dropped *did* contribute to the fit and so cannot be omitted.

For the case of $z = 0.98$, $F = 0.26$. This value of F with $2 = k - g$ and $19 = N - (k + 1)$ degrees of freedom is only significant at the 23% probability level, so we accept the hypothesis that the two grain sizes share a common n and Q but differ in prefactor A. For the $z = 0.95$ case we reach a similar conclusion with $F = 1.47$ which is only significant at the 75% probability level [with $2 = k - g$ and $25 = N - (k + 1)$ degrees of freedom]. Therefore, because the stress dependence, n, and apparent activation energy, Q, are the same for large and small grain sizes, we are justified in using the complete data sets for both the $z = 0.98$ and $z = 0.95$ compositions to evaluate the grain size exponents, p.

To evaluate the grain size exponent, p, we rewrite Eq. (1) as

$$\log_e(T\dot{\epsilon}) = \log_e A_1 - p \log_e d + n \log_e \sigma - \frac{Q}{RT} \quad , \qquad (8)$$

and assume that the grain size, d, is equal to the mean linear intercept length, L. Regressing Eq. (8) yields grain size exponent directly. Table I reports the Q and n for this fit for the complete data sets.

To calculate the global apparent activation energy, Q, and stress dependence, n, to the complete set of data in Table III, we can generalize the complete model of Eq. (4) to use four dummy variables and five sets of independent n, Q, and A. After using the same process described above, the simplest reduced model is one that assumes a common n and Q, and independent A's for the five compositions, for a total of seven independent variables. For this case $F = 1.26$ in Eq. (7) which is only significant at the 28% level with $8 = k - g$ and $56 = N - (k + 1)$ degrees of freedom. Evaluating simpler reduced models, created by discarding any of the A's, yields *F*s that are significant. Therefore, the five sets of data (from three compositions and two grain sizes) share a single stress dependence and apparent activation energy, but all have independent prefactors.